Multiscale modeling of the electrostatic coupling between plasma thruster and spacecraft -comparison with Express-A in-flight measurements

Lucas Nicolle, Pierre Sarrailh, Sébastien Hess, Marc Villemant, Laurent Garrigues, Denis Payan

Multiscale modeling of the electrostatic coupling between plasma thruster and spacecraft - comparison with Express-A in-flight measurements

IEPC-2022-297

Presented at the 37th International Electric Propulsion Conference
Massachusetts Institute of Technology, Cambridge, MA USA
June 19-23, 2022

L. Nicolle[1], P. Sarrailh[2], S. Hess[4], M. Villemant[5]
ONERA, Toulouse, 31000, France

L. Garrigues[3]
LAPLACE, Toulouse, 31000, France

D. Payan[6]
CNES, Toulouse, 31000, France

Thruster plume simulations often use a hybrid approach, modeling ions as particles and electrons as a fluid. Nevertheless, the definition of the pressure law in the fluid transport of electrons can be quite challenging. In this paper, the consequence of the pressure law assumption on plasma plume simulation results is deeply analyzed. To validate our approach, modeling outcomes must be compared with experimental results. This has been done through comparisons between simulation results and in-flight data taken from the Retarding Potential Analyzers (RPA) placed on the solar arrays on the Russian geostationary telecommunication satellite Express-A #3. The RPA allows the measurements of ion current at different distances and field of view configurations with regard to the thrusters. In this paper, a new method to couple plasma simulation to an RPA analytical model is presented. It enables to couple a plasma simulation to an advanced analytical RPA probe model, taking into account the effects of misoriented RPA. Results demonstrate that the electron pressure law can significantly affect primary ion trajectories. The results are compared to Express-A RPA data.

I. Nomenclature

n_e = electron density
T_e = electron temperature
α_T = angle between the thruster to RPA direction with respect to the thruster surface normal (outwards)
β_{RPA} = angle between the RPA to thruster direction with respect to the RPA surface normal (outwards)
η_i = thruster ionization rate

[1] Ph. D Student, DPHY-CSE, lucas.nicolle@onera.fr
[2] Head of research unit, DPHY-CSE, pierre.sarrailh@onera.fr
[3] Senior scientist at CNRS, GREPHE group, laurent.garrigues@laplace-tlse.fr
[4] Research scientist, DPHY-CSE, sebastien.hess@onera.fr
[5] Research scientist, DPHY-CSE, marc.villemant@onera.fr
[6] Research engineer, STDI-PS, denis.payan@cnes.fr

II. Introduction

To understand and predict the erosion and electrostatic discharges (ESD) on spacecraft in the presence of a plasma thruster, it is necessary to properly represent the electrostatic coupling between the plume of the thruster and the spacecraft surfaces. Several works have shown that this coupling has a significant impact on the charging mechanism [1] and can enhance the risk for ESD on solar arrays [2], [3]. Erosion and contamination due to charge exchange ions created by the thruster device on sensitive components like solar cell interconnectors can also lead to premature termination of the mission [4]. As the demand pushes for higher power plasma thruster and higher solar arrays bus voltage, those issues are magnified and become a limiting factor for power upscaling [5]. The goal of the plume models is to represent the primary ion beam dynamics and the coupling with the satellite environment. Thus, a plume numerical simulation usually includes the transport of charged particles and neutral atoms (using full Particle-In-Cell (PIC) [6] or hybrid fluid – PIC [1], [7], [8] approaches), the resolution of the Poisson's equation the computation of collisions between particles. To validate thruster plume and spacecraft interaction models, experimental data are needed.

Although large on-ground vacuum chamber allow to study the effect of the plasma thruster far field plume [9], [10], the conditions are different from space because of the presence of backpressure. The environment in the vacuum facility is denser [11] leading to a greater charge exchange collision rate between the primary ion beam and the residual Xe^+ ions in the chamber. The study of the backflow (i.e., the Xe^+ created from charge exchange collisions) is therefore biased. Moreover, due to the presence of the chamber walls, the radial potential drop in the vacuum chamber is also altered. In-flight experiment allows having a representative measurement for model comparisons. In-flight experiment has been conducted on SMART-1 [12], but only a few data are available in the literature and the plasma diagnostic package position only allows to study the backflow, at a single point in space. On the other hand, the Russian geostationary telecommunication satellite Express-A #3 (launched in June 2000) presents a large number of retarding potential analyzer (RPA) measurements, at various locations with respect to the thruster firing axis, allowing a unique in-flight experimental set-up to study the plasma plume. However, the RPA data processing is non-conventional due to the oblique incidence of the plasma beam coming from the thruster. The probe tilt-angle with respect to the plasma drift vector: β_{RPA} (i.e., the angle between the probe normal axis and the probe – thruster axis) is within a range of $2 - 45°$, and therefore, the measurement of the ion current density is not straightforward anymore. To be able to predict RPA measurements, the analytical RPA model from [13] is used and adapted to a PIC simulation.

In this paper, a new approach based on the prediction of in-flight plume current density prediction is shown, allowing to model a plasma thruster, compute the plume dynamics and predict RPA measurement through an RPA model. The prediction of the RPA measurements from different plume models has been analyzed.

III. Express-A in-flight plume measurements

Express-A set-up description

Express-A #3 is equipped with 8 Fakel SPT-100, a well-documented Hall thruster used for station keeping and two RPAs mounted on the solar panels (DRT1, DRT2). The RPA position allows a scan of ion current and ion energy distribution function (IEDF) as the solar arrays rotate. This unique setup is often compared to thruster plume simulation in Space vacuum (see refs. [14,15] and references therein). The spacecraft is also equipped with electric field and pressure sensors alongside with torque measurements induced by the thruster plume studied in other papers [8], [15]. However, in the scope of this paper, only the RPA data will be investigated.

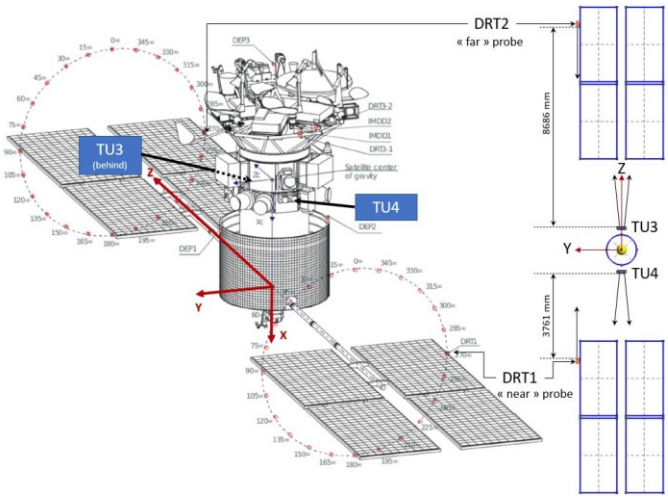

Figure 1 Express-A Thruster and RPA locations [14]

Retarding Potential Analyzer

A retarding potential analyzer is an electrostatic hollow cylindrical probe consisting of three to four polarized grids. The first grid is floating to the same potential as the cylindrical body, restraining the plasma perturbation. The second grid is negatively polarized to -30 to -40 V with respect to the probe floating potential, repelling all the electrons. And finally, the analyzer grid, which potential is sweeping from 0 to 340 V, with respect to the probe floating potential, acting as a high pass filter for the ions. The collected current is then only induced by the ions and decreases as the analyzer grid potential increases.

An RPA measurement can be analyzed in two manners. First, as an ion energy distribution function (IEDF) sensor: if the RPA is oriented toward the studied source, the derivative of the collected current with respect to the analyzer sweeping voltage is proportional to the IEDF in front of the RPA (up to a sign and after correcting for the RPA floating potential induced shift). Second, the RPA current measurement when the analyzer potential is at the probe floating potential can be used as an ion current density measurement. However, the geometry of the RPA and the grids transparencies must be taken into account to apply a correcting factor to the collected current to deduce the true current density.

In this study, only the second type of measurement has been analyzed. The RPA model from [13] has been used to model the ion loss at RPA walls, the repelled ions and the grid transparency.

The RPAs mounted on Express-A are not oriented toward the thruster and therefore, it has been demonstrated in [13] that it is mandatory to take into account the tilt-angle of the RPA (β_{RPA}) to analyze Express-A RPA data.

Note that, in this study, the simulation and in-flight experiment results have been compared in raw current because the correcting factor to pass from raw data to current density is not easy to obtain. Although the technical reports give a constant probe equivalent surface, corresponding to the product of the grid transparencies by the collector area, but the reality is more complex. This equivalent surface depends highly on the angle of the ion flux with respect to the RPA surface normal and on the ion energy. For example, if the RPA is tilted at 45° with respect to the incoming flux direction, it appears clearly that the collection will be highly affected and that the effective surface area will be well below the value from the technical report. Moreover, for a tilted probe, the effective area will be lower if the beam energy increases as the proportion of ions hitting the RPA walls will increase. Indeed, the deflection occurring in the RPA induced by the strong axial electric fields tends to change the ions' velocity vector. For example, if the cut-off grid potential was $-\infty$ in a tilted RPA, the ions would be deviated toward a purely axial trajectory. As low energy ions are more deflected than high energy ions (under the same electric fields), a beam energy increase means a lower equivalent surface.

IV. Simulation method

General approach

To simulate the Express-A RPA response, a model chain approach is used. First, an ion energy distribution function at the thruster exit was computed using a hybrid Hall thruster model for nominal conditions of the SPT-100 [17]. Next, the plasma simulation is handled using the SPIS [1] spacecraft – plasma interaction software, allowing to

model the plasma dynamics in the plume. The thruster ions are modeled as numerical particles, using a PIC approach and the thruster electrons are modeled as a fluid. This software also allows to compute the spacecraft electrical circuit, to model the charge exchange collisions and the plasma surface interactions. As the goal of this paper is to study the effect of the plume model on the RPA response on-board Express-A, several thruster ionization rate η_i and different models will be analyzed for different electron pressure laws. This has been done by closing the electron fluid equation system with a polytropic law and modifying its polytropic index. The law states the relationship between the electron pressure p_e and density n_e as $p_e n_e^{-\gamma} = cst$. This law makes it possible to model an adiabatic expansion (if $\gamma = 5/3$) to an isothermal expansion (if $\gamma = 1$). Previous work has shown that the γ parameter from comparison with an experiment in a vacuum chamber [18] must be between 1.26 and 1.31. Therefore, two different values of γ representing extreme cases have been tested in this study: one case close to isothermal ($\gamma = 1.1$) and the other case, taking the adiabatic expansion ($\gamma = 5/3$).
Finally, to couple the plasma simulation with an RPA probe model, the analytical RPA probe model described in [13] has been implemented in SPIS making it possible to take into account the tilt-angle between the orientation of the RPA and the RPA to thruster direction. However, in the SPIS software, as the ion transport is described with a PIC method using statistical sampling of the ion velocity distribution function using numerical macroparticles, the RPA probe model has been adapted to ensure compatibility. The next section describes the adaptation required to couple the analytical RPA model to PIC ions.

RPA model adaptation to PIC particle detection

Contrary to the analytical description of the simplified transport (without plasma) used in [13], the complex plasma dynamic is captured using numerical particles. If a numerical particle is collected at the entrance of the RPA, a transfer function is applied to its weight, knowing its velocity vector. Its contribution to the total current is computed and accounted for. The total collected current is then a sum over all the particles reaching the collector and not an integration of a continuous velocity phase space, as in [13].
Nevertheless, the issue with the numerical particles approach is that, for the collected current to be representative, a large number of numerical particles have to reach the RPA collector (and so, the RPA entrance). To increase the statistics on the RPA, a backtracking algorithm optimized by octree has been used.

Backtracking and octree optimization

As stated, the difficulty of the coupling between the RPA analytical model and the PIC approach for ions is to obtain a sufficient number of numerical particles on the RPA entrance surface to be able to construct the ion velocity distribution function at the entrance of the probe. In the PIC algorithm, numerical particles are sampled on a source surface, like the thruster exit or simulation environment boundaries. They can also be generated in volume through charge exchange collisions for instance. However, with this approach, a very small number of numerical particles reach the RPA entrance during a simulation. To enhance the collection, the classical PIC approach is coupled with a backtracking algorithm. First, the forward tracked particles (conventional PIC approach) are used to compute the potential map in the simulation (through the PIC algorithm). When a measurement needs to be done, virtual numerical particles are sampled on the RPA entrance surface and are backtracked.
In this approach, we consider two kinds of ions: the thruster ions, created and sampled on the physical thruster exit simulation boundary, and the charge exchange ions, created in volume. The first ions are backtracked until they reach a simulation boundary. If the boundary is the thruster and the energy of the particle can be sampled, then, its probability of sampling (given by the IEDF in volume) is computed and assigned to its weight.
For the second ions (CEX), the weight is computed along trajectory by adding the probability of ion creation in each simulation tetrahedron. This probability depends on the CEX creation rate $\nu_{CEX} = n_n n_i \sigma_{n-i} v_{n-i}$, with n_n and n_i the Xe and Xe^+ density, σ_{n-i}, the $Xe^+ - Xe$ cross-section and v_{n-i}, the relative velocity between ion and neutral.
The main advantage of backtracking is that all the followed particles are known to reach the RPA. When the source is much larger than the RPA entrance surface, backtracking makes it possible to save a lot of computation time.
To backtrack efficiently the particles emitted from the thruster, an optimization is made to sample particles that are emitted from the thruster exit. To do so, an octree-based algorithm splits the velocity phase space at the RPA entrance and the velocity vector of the virtual numerical particles is sampled in preferred directions. The directions of interest are defined by a function targeting directions where particles exist, induce a significant current on the RPA collector, and also in directions where the dispersion of the particle weights on source surfaces is important. This function takes into account the RPA transfer function as well, to optimize the collected current on the RPA collector surface.
To conclude, this optimization combined with the backtracking approach makes it possible to get a smooth ion energy distribution function at the RPA entrance and therefore, to get a low-noise RPA collected current prediction.

V. Simulation

The geometry for the plasma simulation is shown in Figure 2. It consists of a plasma thruster similar to an SPT-100 with an annular exit channel (inner radius $r_i = 0.03m$, outer radius $r_o = 0.05m$). A refinement box in the thruster exhaust area and a cylindrical external boundary box (length $l_{cyl} = 12m$, diameter $d_{cyl} = 10m$). The disk of the external boundary cylinder unexposed to the thruster plume is set as a spacecraft surface (red line, Figure 2) and the other surfaces of the external cylinder are set to open boundaries (black lines, Figure 2), allowing particles to be injected and lost through the surfaces. To solve the Poisson equation, the Space external boundaries are modeled with Fourier-Robin boundary conditions.
The spacecraft charging mechanism is modeled by setting a potential gap between the spacecraft body and the thruster exit at $5T_e$ and in this case, $T_e = 5eV$.
A Geostationary Earth Orbit (GEO) environment is injected at the external boundaries. However, it does not induce a significant effect on the RPA current collection.

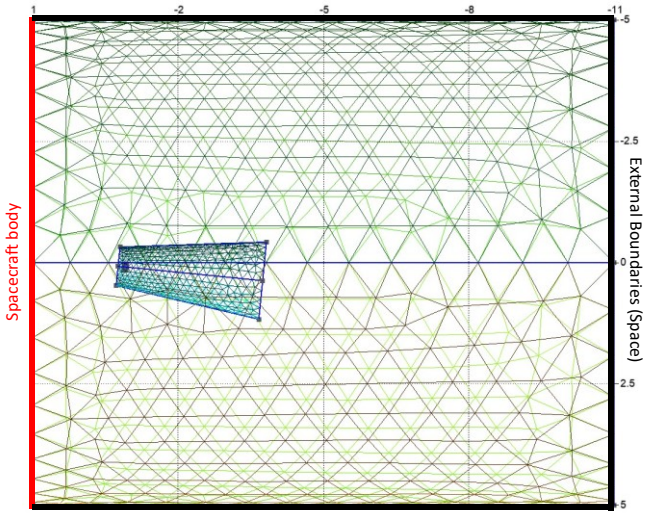

Figure 2 Simulation mesh: A plasma thruster in a cylindrical box

The particles emitted from the thruster are modeled using a hybrid approach, with Xe^+ modeled as numerical particles and electrons as fluid as stated previously.

The RPA current collection is evaluated using the method described in section IV as soon as the simulation is converged (i.e., the time evolution of the current is stable implying that the potential map does not evolve anymore). To have enough RPA current data points, 38 probe locations are evaluated per simulation. All the RPA configurations are available in **Error! Reference source not found.**, in the appendix section.

VI. Results

Effects of the electron cooling model on RPA current collection
In this section, we present the effect of the electron cooling model (i.e., the effect of the electron pressure law) on the ion trajectories. To compare numerical simulation to Express-A RPA, the collected current at the RPA collector is directly evaluated using the model described in [13]. Additionally, to represent the probe collected current as a function of the angle between the thruster normal and the direction of the RPA (α_T), the data are normalized at 1m from the thruster exit using a $1/r^2$ decay law.
The results are split into two figures: Figure 3 shows the current collected by the far probe (DRT2) while Figure 4 shows the current collected by the near one (DRT1). In both figures, the data from Express-A are in black, blue crosses represent the predicted collected current when no plasma model is considered (straight line ion trajectories) and

orange, green and red crosses are the current predicted using a polytropic law for electrons with a polytropic index respectively 1.1 (near isothermal), 1.25 (intermediate case) and $5/3$ (adiabatic).

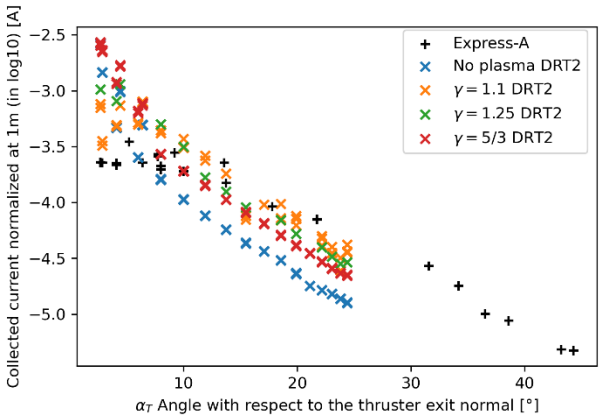

Figure 3 Angular profile of the thruster Xe^+ current collected by the far RPA probe for different polytropic index (in log10) [A]. Data normalized at 1m with a $1/r^2$ law. $T_e = 5eV$, $\eta_i = 95\%$

The far probe current shown in Figure 3 demonstrates that the electron model affects the angular dependency of the predicted current. Indeed, without considering plasma effects (blue crosses), the beam is more focused in the direction of the thruster exit surface normal and therefore, the angular decay of the beam current is significant. However, when a plasma is considered and as the polytropic index tends towards the 1, the effect of the electron pressure in the center of the beam is increased leading to a deflection of ion trajectories and a wider beam. It can be assessed that at $\approx 9m$ from the thruster exit, the electron pressure model has a direct effect on the thruster beam divergence. Therefore, it has to be taken into account when performing such simulations. Moreover, Express-A data showed a good agreement with the isothermal case.

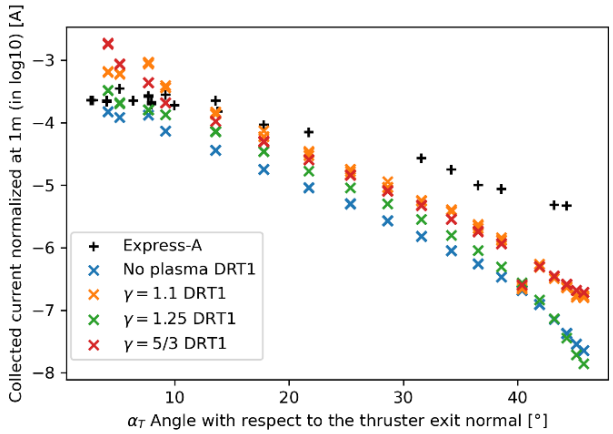

Figure 4 Angular profile of the thruster Xe^+ current collected by the near RPA probe for different polytropic index (in log10) [A]. Data normalized at 1m with a $1/r^2$ law. $T_e = 5eV$, $\eta_i = 95\%$

On the other hand, the simulation of the near probe collected current also shows an effect of the electron model on the RPA current predictions. However, at high angles, the predicted collected current underestimates the observation and no reasonable electron law allows to match the experimental data. To explain this gap, the hypothesis of the CEX current being greater than estimated here is under study. Indeed, the presence of solar array surfaces can attract the CEX, increasing the collected current at its edges**.** One other hypothesis is that the primary ions could have a slightly different angular distribution, and be more divergent than assessed in this study.

Figure 5 shows the collected current for $\gamma = 1.25$, $T_e = 5$eV and $\eta_i = 95\%$ for the CEX (green), the primary ions (orange), and the sum of the two species (blue crosses, hidden behind orange crosses). As we see, the CEX participation in the RPA current is orders of magnitude under primary ions.

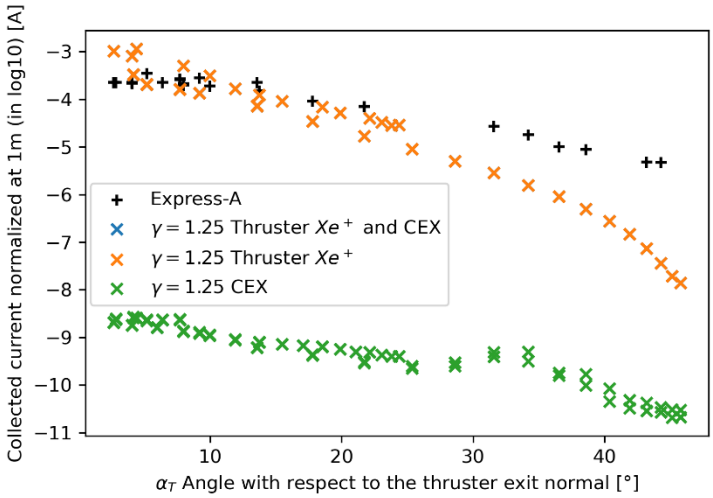

Figure 5 Angular profile of the thruster Xe^+ current collected by the RPA probes for different ion species (in log10) [A]. Data normalized at 1m with a $1/r^2$ law. $T_e = 5eV$, $\eta_i = 95\%$

Effects of the ionization rate on the RPA current collection

The ionization rate η_i impacts the CEX density, the effect can be evaluated taking two cases: a first case where $\eta_i = 95\%$ (efficient Hall thruster) and another case where $\eta_i = 85\%$ (weak ionization performances). The results are shown in Figure 6, for DRT1 and DRT2 at solar arrays angles equal to 0°, 40° and 90°.

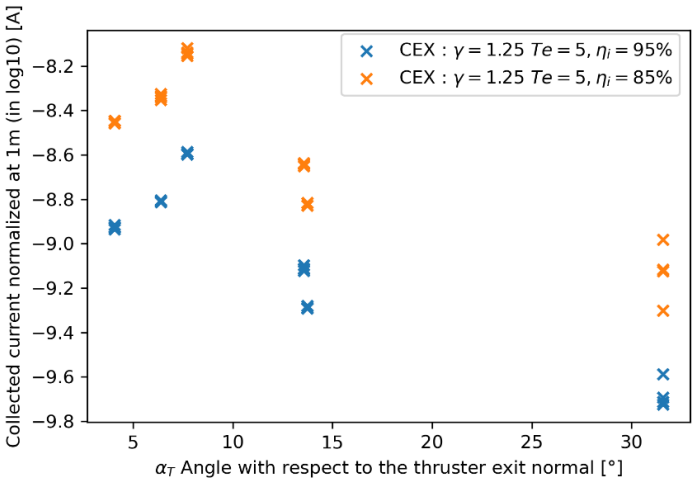

Figure 6 Angular profile of the thruster Xe^+ current collected by the RPA probes for different ionization rates (in log10) [A]. Data normalized at 1m with a $1/r^2$ law. $T_e = 5eV$, $\gamma = 1.25$

As expected, decreasing the ionization performances leads to a higher density of CEX and therefore a higher collected CEX current. However, even in the weak performance case, the CEX current stays orders of magnitude under the primary ions current, even at high α_T angles.

Appendix

Table 1 RPA configurations

Solar array angle / Solar array symmetry [°]	Thruster / thruster symmetry	RPA probe	α_T, angle with respect to thruster [°]	RPA tilt-angle β_{RPA} [°]	Distance thruster – RPA [m]
0 / 0	T4 / RT4	DRT1	7.72	3.38	3.82
	RT3 / T3	DRT2	6.39	1.24	8.74
10 / 350	T4 / RT4	DRT1	4.19	4.85	3.82
	RT3 / T3	DRT2	4.41	1.94	8.74
20 / 340	T4 / RT4	DRT1	5.19	9.21	3.86
	RT3 / T3	DRT2	2.85	3.92	8.76
30 / 330	T4 / RT4	DRT1	9.20	13.79	3.92
	RT3 / T3	DRT2	2.69	5.99	8.78
40 / 320	T4 / RT4	DRT1	13.57	18.19	4.01
	RT3 / T3	DRT2	4.08	8.03	8.82
50 / 310	T4 / RT4	DRT1	17.79	22.29	4.12
	RT3 / T3	DRT2	5.98	10.00	8.87
60 / 300	T4 / RT4	DRT1	21.73	26.03	4.24
	RT3 / T3	DRT2	7.99	11.88	8.93
70 / 290	T4 / RT4	DRT1	25.34	29.4	4.37
	RT3 / T3	DRT2	9.97	32.38	8.99
80 / 280	T4 / RT4	DRT1	28.62	32.38	4.51
	RT3 / T3	DRT2	11.9	15.29	9.06
90 / 270	T4 / RT4	DRT1	31.57	35.00	4.65
	RT3 / T3	DRT2	13.74	16.81	9.13
100 / 260	T4 / RT4	DRT1	34.2	37.28	4.79
	RT3 / T3	DRT2	15.46	16.81	9.19
110 / 250	T4 / RT4	DRT1	36.53	39.22	4.92
	RT3 / T3	DRT2	17.07	19.4	9.26
120 / 240	T4 / RT4	DRT1	38.58	40.87	5.04
	RT3 / T3	DRT2	18.55	20.47	9.33
130 / 230	T4 / RT4	DRT1	40.36	42.23	5.15
	RT3 / T3	DRT2	19.89	21.39	9.43
140 / 220	T4 / RT4	DRT1	41.9	43.32	5.24
	RT3 / T3	DRT2	21.09	22.15	9.43
150 / 210	T4 / RT4	DRT1	43.2	44.17	5.31
	RT3 / T3	DRT2	22.14	22.75	9.47
160 / 200	T4 / RT4	DRT1	44.27	44.79	5.37
	RT3 / T3	DRT2	23.04	23.19	9.5
170 / 190	T4 / RT4	DRT1	45.12	45.17	5.41
	RT3 / T3	DRT2	23.79	23.47	9.52
180 / 180	T4 / RT4	DRT1	45.75	45.34	5.42
	RT3 / T3	DRT2	24.37	23.6	9.53

Acknowledgments

L. Nicolle benefits from an ONERA and CNES Ph.D. grant.

References

[1] P. Sarrailh, S. L. Hess, and J.-C. Mateo-Velez, "Simulations of plasma thruster effect on the electrostatic behavior of spacecrafts in GEO," presented at the AIAA SPACE 2015 Conference and Exposition, Pasadena, California, Aug. 2015. doi: 10.2514/6.2015-4640.

[2] K. H. Wright, T. A. Schneider, J. A. Vaughn, V. V. Funderburk, F. Wong, and G. Gardiner, "Age Induced Effects on ESD Characteristics of Solar Array Coupons After Combined Space Environmental Exposures," presented at the 12th Spacecraft Charging Technology Conference, Kitakyushu, Japan, 2012.

[3] J. J. Likar, A. L. Bogorad, T. R. Malko, N. E. Goodzeit, J. T. Galofaro, and M. J. Mandell, "Interaction of Charged Spacecraft with Electric Propulsion Plume: On Orbit Data and Ground Test Results," *IEEE Trans. Nucl. Sci.*, vol. 53, no. 6, pp. 3602–3606, Dec. 2006, doi: 10.1109/TNS.2006.885107.

[4] L. Yan, P.-Y. Wang, Y.-H. Ou, and X.-L. Kang, "Numerical Study of Hall Thruster Plume and Sputtering Erosion," *J. Appl. Math.*, vol. 2012, pp. 1–16, 2012, doi: 10.1155/2012/327021.

[5] M. Reza, F. Faraji, and T. Andreussi, "Characterization of a high-power Hall thruster operation in direct-drive," *Acta Astronaut.*, vol. 178, pp. 392–405, Jan. 2021, doi: 10.1016/j.actaastro.2020.09.008.

[6] K. Shan, Y. Chu, Q. Li, L. Zheng, and Y. Cao, "Numerical Simulation of Interaction between Hall Thruster CEX Ions and SMART-1 Spacecraft," *Math. Probl. Eng.*, vol. 2015, pp. 1–8, 2015, doi: 10.1155/2015/418493.

[7] T. Muranaka and Y. Inanaga, "Development of a Numerical Tool for Hall Thruster Plume and Spacecraft Interaction Analysis," *Trans. Jpn. Soc. Aeronaut. SPACE Sci. Aerosp. Technol. Jpn.*, vol. 16, no. 5, pp. 366–373, 2018, doi: 10.2322/tastj.16.366.

[8] I. G. Mikellides, Jongeward, Gary A., B. M. Gardner, I. Katz, M. J. Mandell, and V. A. Davis, "A Hall-Effect Thruster Plume and Spacecraft Interactions Modeling Package," presented at the 27th International Electric Propulsion Conference, Pasadena, California, USA, 2001.

[9] G. Giono *et al.*, "Non-Maxwellian electron energy probability functions in the plume of a SPT-100 Hall thruster," *Plasma Sources Sci. Technol.*, vol. 27, no. 1, p. 015006, Dec. 2017, doi: 10.1088/1361-6595/aaa06b.

[10] S.-W. Kim and A. D. Gallimore, "Plume Study of a 1.35-kW SPT-100 Using an ExB Probe," *J. Spacecr. Rockets*, vol. 39, no. 6, pp. 904–909, Nov. 2002, doi: 10.2514/2.3897.

[11] A. Passaro, A. Vicini, and L. Biagioni, "Plasma Thruster Plume Simulation: Effect of Vacuum Chamber Environment," presented at the 35th AIAA Plasmadynamics and Lasers Conference, Portland, Oregon, Jun. 2004. doi: 10.2514/6.2004-2357.

[12] D. M. Di Cara and D. Estublier, "Smart-1: An analysis of flight data," *Acta Astronaut.*, vol. 57, no. 2–8, pp. 250–256, Jul. 2005, doi: 10.1016/j.actaastro.2005.03.036.

[13] L. Nicolle, P. Sarrailh, L. Garrigues, S. Hess, and M. Villemant, "Modelling of a retarding potential analyzer and comparison with Express-A in-flight measurements," *Front. Phys., under review*.

[14] D. Manzella, R. Jankovsky, F. Elliott, I. G. Mikellides, G. A. Jongeward, and D. Allen, "Hall Thruster Plume Measurements On-board the Russian Express Satellites," presented at the 27th International Electric Propulsion Conference, Pasadena, California, USA, 2001. [Online]. Available: http://citeseerx.ist.psu.edu/viewdoc/download;jsessionid=505965F4BFAC7A689E0E7A4C589B9ADC?doi=10.1.1.618.6148&rep=rep1&type=pdf

[15] I. G. Mikellides, G. A. Jongeward, I. Katz, and D. H. Manzella, "Plume Modeling of Stationary Plasma Thrusters and Interactions with the Express-A Spacecraft," *J. Spacecr. Rockets*, vol. 39, no. 6, pp. 894–903, Nov. 2002, doi: 10.2514/2.3896.

[16] I. Boyd, "Hall thruster far field plume modeling and comparison to Express flight data," presented at the 40th AIAA Aerospace Sciences Meeting & Exhibit, Reno, NV, U.S.A., Jan. 2002. doi: 10.2514/6.2002-487.

[17] L. Garrigues, G. J. M. Hagelaar, C. Boniface, and J. P. Boeuf, "Anomalous conductivity and secondary electron emission in Hall effect thrusters," *J. Appl. Phys.*, vol. 100, no. 12, p. 123301, Dec. 2006, doi: 10.1063/1.2401773.

[18] M. Merino *et al.*, "Collisionless electron cooling in a plasma thruster plume: experimental validation of a kinetic model," *Plasma Sources Sci. Technol.*, vol. 29, no. 3, p. 035029, Mar. 2020, doi: 10.1088/1361-6595/ab7088.